Improving Transient Stability of Power Synchronization Control for Weak Grid Applications

Sepehr, Amir; Pouresmaeil, Mobina; Hojabri, Mojgan; Blaabjerg, Frede; Pouresmaeil, Edris

Published in:
Proceedings of the 2020 IEEE 21st Workshop on Control and Modeling for Power Electronics (COMPEL)

DOI (link to publication from Publisher):
10.1109/COMPEL49091.2020.9265786

Publication date:
2020

Document Version
Accepted author manuscript, peer reviewed version

Improving Transient Stability of Power Synchronization Control for Weak Grid Applications

Amir Sepehr, Mobina Pouresmaeil
Dept. of Elec. Eng. and Automation
Aalto University
Espoo, Finland
amir.sepehr@aalto.fi
mobina.pouresmaeil@aalto.fi

Mojgan Hojabri
Dept. of Elec. Eng. (IET)
Lucerne University of Applied Science and Arts
Lucerne, Switzerland
mojgan.hojabri@hslu.ch

Frede Blaabjerg
Dept. of Energy Technology
Aalborg University
Aalborg, Denmark
fbl@et.aau.dk

Edris Pouresmaeil
Dept. of Elec. Eng. and Automation
Aalto University
Espoo, Finland
edris.pouresmaeil@aalto.fi

***Abstract*— Power synchronization control (PSC) has a promising potential to be used in interface converters of large-scale renewable generations operating under weak-grid condition. This paper presents a modified PSC-based control structure that provides an enhanced dynamic response, reinforced synchronization, and reduced vulnerability against grid transients. By utilizing a back-calculation scheme, the active power reference in the synchronization loop of PSC is configured to be adapted to the grid transients for avoiding loss of synchronization (LOS). Furthermore, the proposed control structure prevents power-injection collapse (PIC) and mitigates the dc current components of the converter caused by transients in weak grids. Performance and feasibility of the proposed control structure are highlighted and verified by simulation of various scenarios and operating conditions.**

Keywords*— *interface converter, power synchronization control, solid fault, transient angel stability, weak grid.

I. INTRODUCTION

Transition to a sustainable society necessitates energy generation in distributed nodes and even weak grids. In terms of power system stability and converter control system design, a weak grid can be described as a power system where the short circuit ratio (SCR) at the point of common coupling (PCC) is low and significant frequency fluctuation is possibly expected as a consequence of insufficient total system inertia [1]-[3]. In other words, a weak grid comes along with voltage fluctuations at the PCC followed by unbalanced and/or distorted voltage waveforms [3], [4].

Mainly, voltage-source converters (VSCs) are the common products used in converter-interfaced renewables (CIRs) [1], [5]. The majority of CIRs are designed to function as current-controlled grid-feeding converters [1]. The grid-feeding converter controls the injected current through a vector current-control structure on the basis of a voltage-dependent synchronization, typically a synchronous reference frame phase-locked loop (SRF-PLL) [2], [6]. Utilizing PLL for synchronization with weak electric grids may cause synchronization instability which is characterized by oscillations of the converter's frequency and power [6], [7]. The synchronization instability severely degrades the quality of the delivered power and in the same way, hinders providing supportive services including grid voltage support and virtual inertia provision [3], [4], [8].

Accordingly, to address the negative impact of PLL on the CIRs under weak-grid condition, power synchronization control (PSC) has been developed [9]-[11]. PSC facilitates converter operation with ultraweak grids and provides more robust small-signal stability than that of vector current control [9]-[11]. Small-signal stability of PSC has been studied through Jacobian transfer matrix and impedance models [10], [12]. Similarly, transient stability of PSC has been studied based on design-oriented transient stability analysis and time-domain simulation in [12]-[15]. Although the conducted researches provide insight into the stability of PSC, solutions for improving PSC transient stability is hitherto unaddressed. In addition, the transient response of PSC is different from that of a synchronous generator (SG) in three main aspects:

a) Virtual inertia is not embedded in PSC and the time constant of PSC is less than that of an SG [10].

b) The converter current is limited to 1.2-1.6 p.u. whereas an SG is capable of current injection up to 6-8 p.u. [16].

c) PSC exhibits a non-minimum-phase behavior that means the active power goes down before it responds to the positive change in the power angle [9], [10].

Therefore, this paper intends to present solutions for improving PSC transient stability against grid faults as well as reducing the risk of loss of synchronization (LOS) and power-injection collapse (PIC). In this way, the main contributions of this paper are as follows:

a) The deteriorative effect of nonminimum-phase behavior and the limited bandwidth of PSC are considered in the transient angle stability analysis under weak grid condition.

b) An enhanced control structure is proposed by utilizing a back-calculation scheme, in which the active power reference in the synchronization loop of PSC is configured to be adapted to the grid condition.

c) The enhanced control structure guarantees dc-component suppression in the phase currents of PSC-controlled converters during transients.

The rest of this paper is organized as follows. The principles of PSC and the studied control system are reviewed in Section II. Section III discusses the transient stability of PSC during transients in weak grids. Then, the enhanced

control structure is introduced in Section IV. Section V demonstrates the performance of the enhanced control structure during transients and grid fault events. Conclusions are summarized in Section VI.

II. Power Synchronization Control (PSC)

The description of PSC for a grid-connected voltage-source converter is presented in detail in [9], and [10]. PSC control structure is shown in Fig. 1, where active power control and synchronization with the ac system are performed through power synchronization loop (PSL) given by

$$\theta_{ref} = K_{ip}\int (P_{ref} - P_{pcc}) + \omega_0 t \tag{1}$$

$$\delta = \theta_{ref} - \theta_g = K_{ip}\int (P_{ref} - P_{pcc}) \tag{2}$$

where θ_{ref} and K_{ip} are the generated phase angle and the integral gain of PSL, respectively. P_{ref} is the active power reference, P_{pcc} is the measured output active power at the PCC, and ω_0 denotes the grid frequency. θ_g is the phase angle of the infinite bus voltage and its initial value is assumed to be zero, i.e., $\theta_g = \omega_0 t$. Power angle δ is the phase difference between the voltage at the PCC and the infinite bus voltage. Alternating voltage and reactive power are controlled by adjusting the additional internal-voltage ΔV given by

$$\Delta V = K_{iv}\int (U_{ref} - U_{pcc}) \tag{3}$$

where K_{iv} is the integral gain of the controller, U_{ref} is the PCC voltage-reference amplitude, and U_{pcc} is the measured-voltage amplitude at the PCC. In order to provide damping against potential resonances, converter voltage-reference vector $\mathbf{V}_{ref}^{dq}$ in synchronous reference frame (SRF) is generated by the voltage-vector control law, which is expressed by

$$\mathbf{V}_{ref}^{dq} = (V_0 + \Delta V) - H(s)\mathbf{i}^{dq} \tag{4}$$

$$H(s) = \frac{k_d s}{s + \omega_d} \tag{5}$$

where, V_0 is the nominal voltage, $\mathbf{i}^{dq}$ is the converter current vector in SRF, and $H(s)$ is a high-pass filter for obtaining damping in which k_d and ω_d are the gain and bandwidth of the high-pass filter, respectively. Further, a backup PLL is embedded in the control system for smoothing initial synchronization with the grid and obtaining current-limiting capability during severe grid faults where switching to the current-control mode is necessary, described in detail in [10]-[12]. Linearized dynamic model that relates the change in the active power ΔP due to the change in the load angle $\Delta\theta$ can be expressed by $J_{P\theta(s)}$ as:

$$J_{P\theta(s)} = \frac{\Delta P}{\Delta \theta}. \tag{6}$$

The transmission zeros of $J_{P\theta(s)}$ limit the achievable bandwidth of the control system which are dependent on the operating point of the converter as described in [9], [10]. The specific situation in which the zeros reach to the origin is when

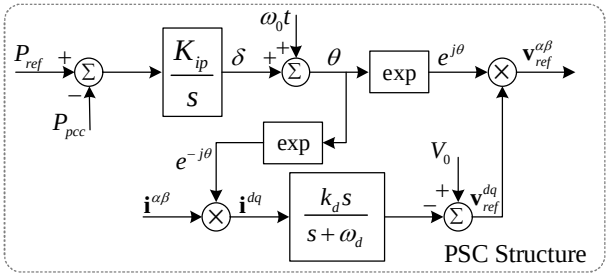

Fig. 1. Block diagram of PSC structure.

$\delta = \pm\pi/2$; whereas, in order to achieve sufficient bandwidth and gain, operating close to $\delta = \pm\pi/2$ is not recommended.

III. Transient Stability of PSC in Weak Grids

In practice, a converter-interfaced renewable generation is equipped with energy storage for delivering supportive services consisted mainly power quality enhancement and virtual inertia provision. Based on this, a well-regulated dc-link voltage is supposable during transients. As depicted in Fig. 2, the interface converter connects to the infinite bus via the converter output filter L_{filter}, a transformer L_{trans}, and two parallel transmission lines L_{line1} and L_{line2}. Since the shunt capacitances have negligible impacts on the transient stability of the system, the converter output filter and the two transmission lines are modelled by inductances [14]. In the assumed control system, the converter supports the PCC voltage and regulates the injected active power into the grid. This assumption is based on the characteristics of high-impedance weak grids where during high-impedance solid faults the converter can support the PCC voltage without the risk of overcurrent. In this case, the amplitude of the converter voltage is fixed at the maximum allowed value. The dynamic representation of PSC can be expressed by a first-order nonlinear equation as:

$$L_T = L_{filter} + L_{trans} + L_{line1} \,||\, L_{line2} \tag{7}$$

$$\dot{\delta} = K_{ip}\left(P_{ref} - \frac{3U_{pcc}U_{bus}}{2\omega_0 L_T}\sin\delta\right) \tag{8}$$

where L_T denotes equivalent inductance of the system and U_{bus} represents the infinite bus voltage-amplitude. The equivalent inductance of the system defines the SCR value of the grid. The SCR imposes limitations on both the maximum reachable generated active-power and PSC transient stability which are primarily affected by the weak-grid operating condition. Weak-grid operating condition requires a higher value of the power angle than that of a strong-grid operating condition. In addition, the gain and bandwidth of PSC is dependent on the power angle and the operating point of the converter. As the power angle is increased, the gain and bandwidth of PSC is decreased. Thus, following a large disturbance in a weak grid the PSC transient stability is contingent on the dynamic response of the power angle.

In this study, a symmetrical three-phase to ground high-impedance fault in a weak grid is considered (as shown in Fig. 2) where the control system does not switch to the vector current control. The circuit breakers of the transmission line 2 trip and clear the fault in a certain time-period, and the SCR of the grid reduces significantly. Following the fault, the system achieves a new stable equilibrium point if the power

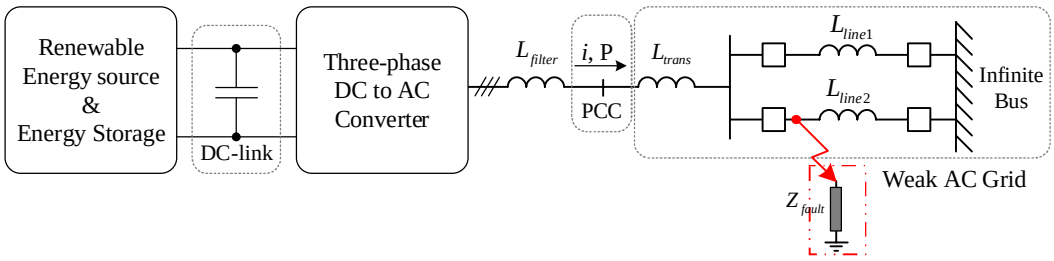

Fig. 2. Converter-interfaced renewable-generation connected to a weak ac grid through two transmission lines.

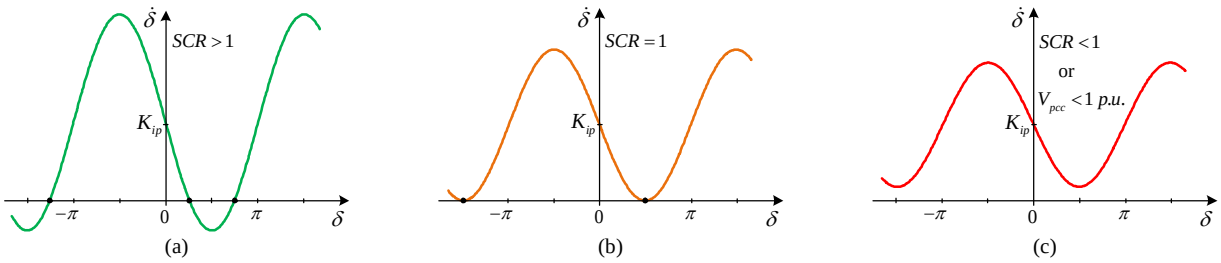

Fig. 3. Phase portraits for the three different PSC dynamics following a solid fault in a weak grid (a) A weak grid with an SCR greater than 1. (b) A very weak grid with an SCR equal to 1. (c) An ultra-weak grid with a PCC voltage less than 1 p.u. or an SCR less than 1.

angle converges to a new value, which is dependent on the pre-fault operating point as well as the SCR value at pre-fault, during-fault, and post-fault operation.

In brief, by assuming active power reference equal to 1 p.u., three different dynamics are expected

a) A stiff or weak grid with an SCR greater than 1.

b) A very weak grid with an SCR equal to 1.

c) An ultra-weak grid with a PCC voltage less than 1 p.u. or an SCR less than 1, which is mostly presumable during fault-period and post-fault operation.

Fig. 3 (a), (b), and (c) demonstrate the phase portraits of the mentioned three different dynamics, respectively. This analysis is based on the parameters listed in Table I and the following assumptions:

a) The converter is controlled by PSC during fault and post-fault condition.

b) The converter output voltage is fixed at the maximum allowed value in order to support the PCC voltage during fault and post-fault condition.

c) The fault impedance is high enough to limit the converter's current contribution below the maximum tolerated value to guarantee uninterrupted operation.

d) Due to the weak grid operating condition, the pre-fault power angle is large enough to reduce the gain and bandwidth of the PSC controller.

In general, depending on the pre-fault operating point of the converter and the during-fault and post-fault grid condition, two different cases for stability problem can be considered. First, a stiff or weak grid with an SCR greater than 1 is available and the system has equilibrium points after the disturbance (as shown in Fig. 3 (a)). Second, there are no equilibrium points or because of the transmission zeros of $J_{P\theta(s)}$, which are placed at $\delta = \pm\pi/2$, transient instability happens (as shown in Fig. 3 (b) and (c)).

A. *Case I: Stable equilibrium points are accessible*

In this case, following a disturbance, stable equilibrium points are present and accessible. As shown in Fig. 3 (a), the disturbance, including the fault occurrence and the fault clearance, leads to an increase in both the SCR and the power angle. Afterwards, the operating point of the converter moves to a new stable equilibrium point where the power angle is less than $\pi/2$.

B. *Case II: Transient instability occurs*

In a close vicinity of $\delta = \pm\pi/2$ the gain and bandwidth of PSC is limited, thus an equilibrium point where the power angle is close to $\pi/2$, does not lead to stable operation following the disturbance. In addition, when the SCR is less than 1 or the PCC voltage is less than 1 p.u., there are no equilibrium points for injecting the rated active power to the grid and the transient instability is unpreventable for the converter controlled by the conventional PSC. The phase portraits of the dynamics regarding to the transient instability are depicted in Fig. 3 (b) and (c).

C. *Analysis and simulation of PSC transient angle stability*

The stability of synchronization in PSC-controlled converters can be lost when the power angle approaches to π and the direction of the active power through the interface converter changes. Once the power angle reaches π, a sharp drop in the injected active power to the grid happens, the active power balance in the dc-link is affected, and consequently the interface converter collapses (also known as PIC). It should be noted that under weak-grid condition, due to the non-minimum phase characteristic of PSC and limited gain and bandwidth, particularly when the operating point is close to $\delta = \pm\pi/2$, the power angle increases faster than that of synchronous generators. The power angle trajectory of the system shown in Fig. 2 is depicted in Fig. 4 (a), where the power angle at the instant of fault clearance is greater than π. Fig. 4 (b) represents the simulation results of the studied system with the parameters listed in Table I. The fault clearance time is set to be equal to five power-system cycle (one hundred milliseconds) to show the strong possibility of transient angle instability as well as LOS and PIC.

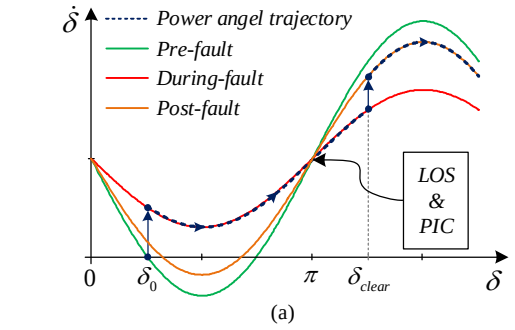

(a)

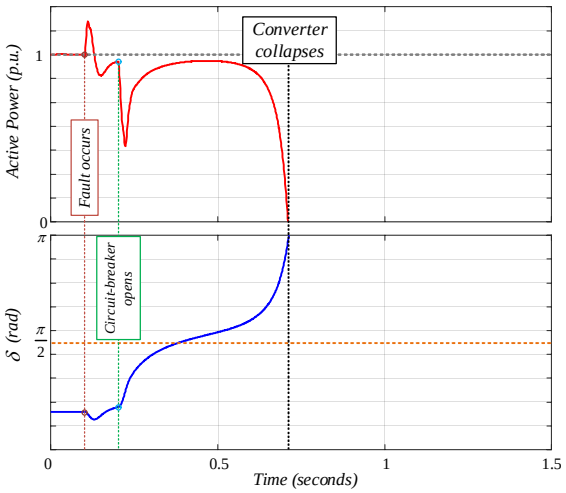

(b)

Fig. 4. (a) Phase portrait of conventional PSC. (b) Active power and power angle trajectory of conventional PSC following a solid fault.

IV. Improving the Transient Angle Stability of PSC

Since the deteriorative effect of the weak-grid operating condition on the transient angle stability of PSC is analyzed, this section aims to propose an enhanced transient stability (ETS) PSC structure in order to prevent the LOS and PIC. When the power angle approaches $\pi/2$, the gain and bandwidth of $J_{P\theta(s)}$ decreases considerably, as a result the control system increases power angle rapidly in order to inject more active power to the grid because the active power reference is greater than the measured active power. Whereas there is no feature in PSC that bounds the power angle. As the active power error is the main reason for unbounded increase of the power angle, by introducing power-angle saturation and active-power back-calculation, the active power reference in PSC is modified and the transient angle stability can be improved.

A. Modified active power error

In normal operating condition, the power angle never reaches $\pi/2$, thus no problem is encountered. However, for large steps in the active-power error due to the grid disturbances, the PSL output signal exceeds critical power-angle δ_{crt}, which is determined based on the lower limits of the bandwidth and gain of the controller. Especially for higher grid impedance and lower post-fault SCR, the power-angle produced by the PSL exceeds the critical power-angle. Therefore, the saturation function, illustrated in Fig. 5, limits the PSL power-angle, and the saturated power-angle $\bar{\delta}$ should be used as the reference to the converter voltage-angle. The saturation function is expressed by

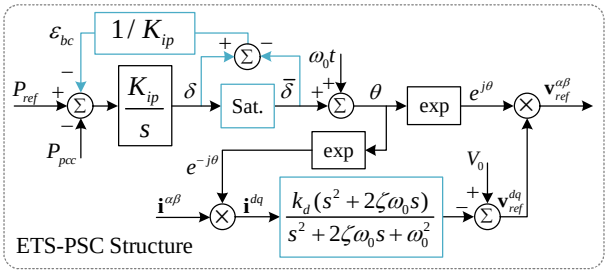

Fig. 5. Block diagram of ETS-PSC structure.

$$\bar{\delta} = sat(\delta, \delta_{crt}) = \begin{cases} \delta_{crt}, & \delta > \delta_{crt} \\ \delta, & -\delta_{crt} \le \delta \le \delta_{crt} \\ -\delta_{crt}, & \delta < -\delta_{crt} \end{cases}. \tag{9}$$

Because of the saturation, the modified PSL contains a nonlinearity and it is important to prevent windup in the PSL. By applying the following back-calculation method, the PSL input is altered from the actual active-power error ε_p to a modified active-power error $\bar{\varepsilon}_p$. The modified PSL can be described as:

$$\begin{aligned} \bar{\delta} &= sat(\delta, \delta_{crt}) \\ \varepsilon_p &= P_{ref} - P_{pcc} \\ \varepsilon_{bc} &= \frac{1}{K_{ip}}(\delta - \bar{\delta}) \\ \delta &= K_{ip}\int \bar{\varepsilon}_p = K_{ip}\int (\varepsilon_p - \varepsilon_{bc}) \end{aligned} \tag{10}$$

where, ε_{bc} represents the effect of the back-calculation method on the modified PSL. In other words, the modified active-power error $\bar{\varepsilon}_p$ is assumed to be such that the saturation operator never is entered and the integrator windup in PSL would not occur. Modifying the active power error by the back-calculation method and calculating the converter voltage-angle θ based on the saturated power-angle reference $\bar{\delta}$, result in ETS-PSC structure which provides an enhanced transient angle stability.

B. Dc current component suppression

PSC structure has a limited gain for suppressing dc current components of the converter caused by transients in high impedance grids. Thus, following any switching or transient in the grid, dc current components decay slowly and occupy the converter's current capacity.

Since PSC-controlled converter behaves as a three-phase balanced voltage source, the converter's contribution in the fault current, during voltage dips on the ac grid, is instantaneous and the converter can deliver the natural instantaneous short-circuit current without delay. Natural instantaneous short-circuit current is the potential current that would be supplied without any current limitation. The fundamental frequency component of the internal balanced three-phase voltage of the converter $e_i(t)$ is given by

$$\begin{aligned} e_i(t) &= \hat{V}\sin(\omega_0 t + \theta_i) \\ i &= a, b, c \end{aligned} \tag{11}$$

where $\hat{V}$ is the internal voltage amplitude of the converter, and θ_i is the internal voltage phase angle of the converter in radian. For a solid three-phase high-impedance short-circuit fault as shown in Fig. 2, the natural short-circuit current is expressed by

$$i_i(t) = \frac{\hat{V}}{|Z_{eq}|}\left\{\sin\left[\omega_0 t + \theta_i - \tan^{-1}\left(\frac{\omega_0 L_{eq}}{R_{eq}}\right)\right] - \sin\left[\theta_i - \tan^{-1}\left(\frac{\omega_0 L_{eq}}{R_{eq}}\right)\right] e^{-t/\left(\frac{L_{eq}}{R_{eq}}\right)}\right\} \quad (12)$$

where Z_{eq} denotes the equivalent fault impedance including converter output filter impedance, transformer impedance, and the fault impedance Z_{fault}. Resistance and inductance of the equivalent fault impedance are represented by R_{eq} and L_{eq}, respectively. The natural fault current consists of a steady-state ac current component and a transient dc current component that decays exponentially with a dc time constant equal to L_{eq}/R_{eq}. Although the grid impedance may be more resistive in low-voltage microgrids, basically the grid impedance and the converter output filter are highly inductive. Consequently, the natural time constant of the decaying dc current component is high enough to cause thermal and overcurrent issues during transients.

In order to suppress the dc current components of the converter and improve fault-ride-through capability of PSC, the high-pass filter $H(s)$ in PSC structure is replaced by $H_{ETS}(s)$ which is defined as:

$$H_{ETS}(s) = \frac{k_d(s^2 + 2\zeta\omega_0 s)}{s^2 + 2\zeta\omega_0 s + \omega_0^2} \quad (13)$$

where ζ determines the suppression capability of the dc current components in the proposed ETS-PSC structure. The defined $H_{ETS}(s)$ provides both damping and dc current component suppression. In the studied system, ζ is considered to be equal to 0.5.

In order to demonstrate the characteristic of the high-pass filter required for providing damping in PSC and ETS-PSC, Fig. 6 shows the bode plot of the transfer function of the high-pass filter in the two cases PSC and ETS-PSC. The two filters have the same attenuation to the low-frequency current components, which are in the synchronous reference frame, however, $H_{ETS}(s)$ has less attenuation to the high-frequency current components. As the current components are derived from the synchronous reference frame, the dc components of the converter phase currents result in higher frequency components in the synchronous reference frame. This means in comparison to $H(s)$, $H_{ETS}(s)$ provides more damping and more virtual resistance in the presence of both dc current components and high-frequency current components. Therefore, by introducing $H_{ETS}(s)$, the damping and dc current component suppression will be improved.

V. Simulation and Evaluation of ETS-PSC

In order to evaluate the transient stability of the ETS-PSC, the studied system shown in Fig. 2 is simulated in MATLAB/Simulink with the parameters listed in Table I. Phase portrait and time-domain simulation for the proposed

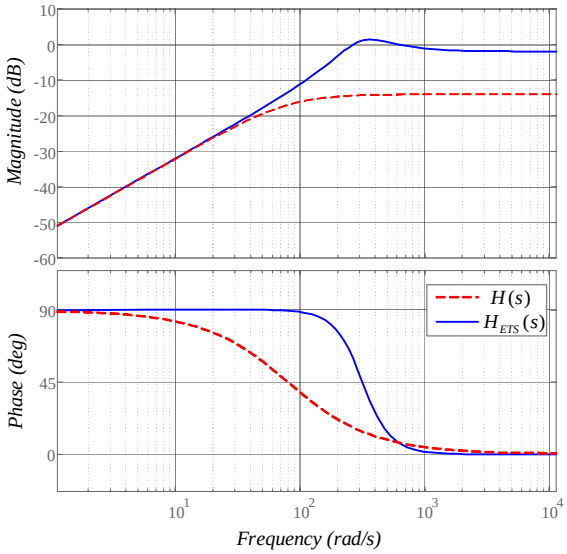

Fig. 6. Bode diagram of the high-pass filter for obtaining damping and dc current component suppression used in PSC and ETS-PSC.

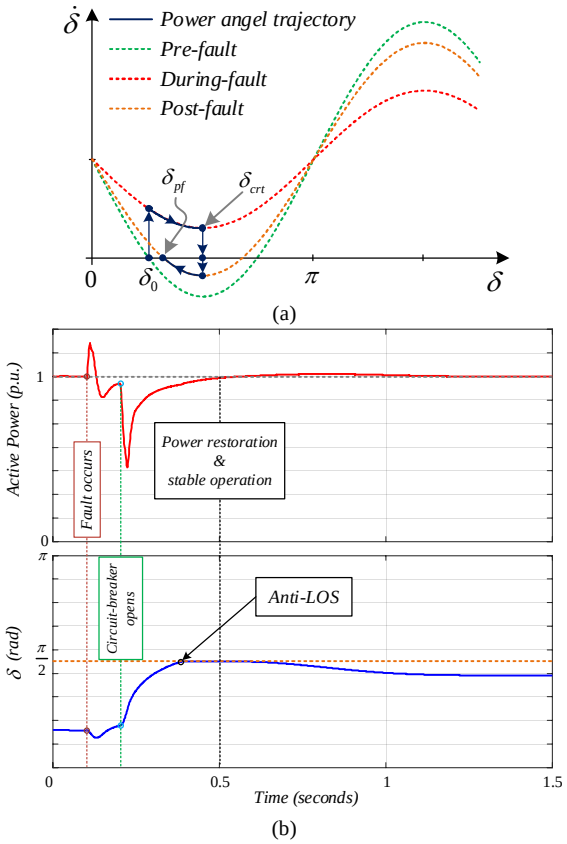

Fig. 7. (a) Phase portrait of ETS-PSC. (b) Active power and power angle trajectory of ETS-PSC following a solid fault.

ETS-PSC are shown in Fig. 7, where the power-angle trajectory of the ETS-PSC and the injected active-power of the converter following a disturbance including high-impedance solid fault and fault clearance under weak grid condition are depicted. As it can be noticed, LOS and PIC would not occur since in the proposed ETS-PSC the active power error and the converter voltage-angle are configured to be adapted to the grid transients. Furthermore, active-power restoration and stable post-fault operation can be achieved by the proposed ETS-PSC structure as shown in Fig. 7 (a) and (b). The power angle is bounded to δ_{crt} and δ_{pf} is the post-fault power angle.

In addition, to evaluate the effectiveness of the proposed high-pass filter, the converter phase currents during the grid disturbance are depicted in Fig. 8. Fig. 8 (a) shows the results for ETS-PSC where the conventional high-pass filter $H(s)$ is used. In this case, the dc current components decay slowly and occupy the converter current capacity. Whereas Fig. 8 (b) shows the results for ETS-PSC where the proposed high-pass filter $H_{ETS}(s)$ is used and dc current components are suppressed properly.

VI. Conclusion

This paper investigated the transient angle stability of PSC by taking the weak-grid operating condition into account. The transient instability of PSC was illustrated and an enhanced transient angle stability control structure was presented. The proposed ETS-PSC provides reinforced synchronization against grid transients by introducing a modified active power error expression and dc current component suppression. Furthermore, ETS-PSC facilitates both post-fault operation of the converter and active-power-delivery restoration by bounding the power angle of the converter and suppressing the dc current component during transients. Time-domain simulations confirmed the ability of ETS-PSC to deliver active power and resynchronize the converter following a solid-fault on a weak grid.

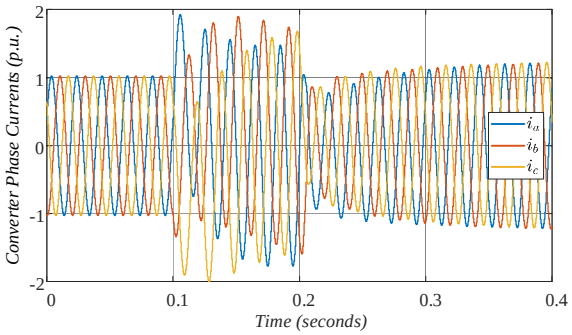

(a)

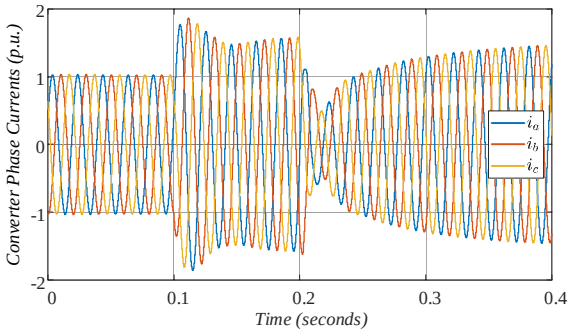

(b)

Fig. 8. Converter phase currents during solid fault (a) ETS-PSC with first-order high-pass filter. (b) ETS-PSC with the modified high-pass filter and dc current component suppression.

TABLE I. Main Parameters of the Studied System

Parameter	Description	Value
L_{filter}	Filter inductance	0.07 p.u.
L_{line1}	Line 1 inductance	0.8 p.u.
L_{line2}	Line 2 inductance	0.8 p.u.
L_{trans}	Transformer inductance	0.057 p.u.
Z_{fault}	Fault impedance	0.5 p.u.
K_{ip}	PSL integrator gain	0.01 p.u.
k_d	High-pass filter gain	0.2 p.u.
ω_d	High-pass filter bandwidth	100 rad/s

References

[1] J. Xu, S. Xie, and T. Tang, "Evaluations of current control in weak grid case for grid-connected LCL-filtered inverter," *IET Power Electron.*, vol. 6, no. 2, pp. 227–234, Feb. 2013.

[2] S. Zhou *et al.*, "An Improved Design of Current Controller for LCL-Type Grid-Connected Converter to Reduce Negative Effect of PLL in Weak Grid," *IEEE J. Emerg. Sel. Top. Power Electron.*, vol. 6, no. 2, pp. 648–663, Dec. 2018.

[3] A. Sepehr, E. Pouresmaeil, M. Saeedian, M. Routimo, R. Godina, and A. Yousefi-Talouki, "Control of Grid-Tied Converters for Integration of Renewable Energy Sources into the Weak Grids," in *Proc. IEEE SEST*, Sep. 2019, pp. 1-6.

[4] M. Zhao, X. Yuan, J. Hu, and Y. Yan, "Voltage Dynamics of Current Control Time-Scale in a VSC-Connected Weak Grid," *IEEE Trans. Power Syst.*, vol. 31, no. 4, pp. 2925–2937, Oct. 2016.

[5] J. Sun, "Impedance-based stability criterion for grid-connected inverters," *IEEE Trans. Power Electron.*, vol. 26, no. 11, pp. 3075–3078, Apr. 2011.

[6] L. Huang *et al.*, "Grid-Synchronization Stability Analysis and Loop Shaping for PLL-based Power Converters With Different Reactive Power Control," *IEEE Trans. Smart Grid*, vol. 11, no. 1, pp. 501-516, June 2019.

[7] S. Ma, H. Geng, L. Liu, G. Yang, and B. C. Pal, "Grid-Synchronization Stability Improvement of Large Scale Wind Farm During Severe Grid Fault," *IEEE Trans. Power Syst.*, vol. 33, no. 1, pp. 216–226, May 2017.

[8] M. Mehrasa, A. Sepehr, E. Pouresmaeil, M. Marzband, J. P. S. Catalao, and J. Kyyra, "Stability analysis of a synchronous generator-based control technique used in large-scale grid integration of renewable energy," in *Proc. IEEE SEST*, Sep. 2018, pp. 1-5.

[9] L. Harnefors, M. Hinkkanen, U. Riaz, F. M. M. Rahman, and L. Zhang, "Robust analytic design of power-synchronization control," *IEEE Trans. Ind. Electron.*, vol. 66, no. 8, pp. 5810–5819, Oct. 2019.

[10] L. Zhang, L. Harnefors, and H. P. Nee, "Power-synchronization control of grid-connected voltage-source converters," *IEEE Trans. Power Syst.*, vol. 25, no. 2, pp. 809–820, May 2010.

[11] S. Mukherjee, V. R. Chowdhury, P. Shamsi, and M. Ferdowsi, "Power-Angle Synchronization for Grid-Connected Converter With Fault Ride-Through Capability for Low-Voltage Grids," *IEEE Trans. Energy Convers.*, vol. 33, no. 3, pp. 970–979, Sep. 2018.

[12] H. Wu and X. Wang, "Design-oriented transient stability analysis of grid-connected converters with power synchronization control," *IEEE Trans. Ind. Electron.*, vol. 66, no. 8, pp. 6473–6482, Aug. 2019.

[13] H. Cheng, Z. Shuai, C. Shen, X. Liu, Z. Li, and Z. John Shen, "Transient Angle Stability of Paralleled Synchronous and Virtual Synchronous Generators in Islanded Microgrids," *IEEE Trans. Power Electron.*, vol. 35, no. 8, pp. 8751–8765, Aug. 2020.

[14] Z. Shuai *et al.*, "Transient Angle Stability of Virtual Synchronous Generators Using Lyapunov's Direct Method," *IEEE Trans. Smart Grid*, vol. 10, no. 4, pp. 4648–4661, July 2019.

[15] M. G. Taul, X. Wang, P. Davari, and F. Blaabjerg, "An Overview of Assessment Methods for Synchronization Stability of Grid-Connected Converters under Severe Symmetrical Grid Faults," *IEEE Trans. Power Electron.*, vol. 34, no. 10, pp. 9655–9670, Oct. 2019.

[16] M. G. Taul, X. Wang, P. Davari, and F. Blaabjerg, "Current Limiting Control with Enhanced Dynamics of Grid-Forming Converters during Fault Conditions," *IEEE J. Emerg. Sel. Top. Power Electron.*, vol. 8, no. 2, pp. 1062–1073, June 2020.